DOI: 10.48011/asba.v2i1.1263

MPC Based Feedback-Linearization Strategy of a Fixed-Wing UAV ⋆

Leonardo A. A. Pereira * **Luciano C. A. Pimenta** ** **Guilherme V. Raffo** **

* *Graduate Program in Electrical Engineering - Universidade Federal de Minas Gerais - Av. Antônio Carlos 6627, 31270-901, Belo Horizonte, MG, Brazil, (e-mail: leonardoaapereira@gmail.com).*
** *Department of Electronic Engineering - Universidade Federal de Minas Gerais - Av. Antônio Carlos 6627, 31270-901, Belo Horizonte, MG, Brazil, (e-mail: lucpim@cpdee.ufmg.br, raffo@ufmg.br).*

Abstract: This work proposes a fixed-wing UAV (Ummaned Aerial Vehicle) control strategy based on feedback-linearization and model predictive control (MPC). The strategy makes use of the relationship between the applied control inputs of the UAV and the generalized forces and moments actuating on it. A linear model is obtained by the exact feedback-linearization technique, followed by the use of MPC to solve the trajectory tracking and the control allocation problems. The proposed controller is capable of actuating on the 6 DOF (Degrees of Freedom) of the UAV, avoiding inherited restrictions when the model is decoupled. The proposed strategy is applied in a curve tracking task. Simulations are performed using MATLAB software, and the results show the efficiency of the proposed control strategy.

Keywords: Fixed-Wing UAV, Feedback-Linearization, Model Predictive Control, Optimal Control Allocation, Vector Fields.

1. INTRODUCTION

As the use of unmanned aerial vehicles (UAVs) has increased, more techniques have been developed concerning path planning, navigation and control. Both military and civilian applications usually require a UAV to be able to estimate its own pose, process the information provided by the environment and follow a given trajectory autonomously.

Some tasks like surveillance, terrain mapping and convoy protection require a long endurance, in terms of energy consumption. Therefore, the use of a fixed-wing UAV is highly recommended due to its greater endurance when compared to multirotors. Nevertheless, the nonlinear behavior of these systems, mechanical constraints, and uncertainties impose challenges in UAV guidance.

Different proposals regarding fixed-wing UAV guidance can be found in the literature. A common solution is to decouple the lateral from the longitudinal dynamics (Espinoza et al., 2014; Beard et al., 2014; Garcia-Baquero et al., 2018). However, this decoupling implies that the UAV is flying in steady-state conditions, as mentioned in (Stevens et al., 2015), which is not the case in many applications which are subject to fast and time-varying reference trajectories.

Another frequently found solution, makes use of lower level controllers, usually PID, which simplifies the complex nonlinear model. This strategy is mostly used in RC (radio controlled) planes (Kang and Hedrick, 2009).

This work deals with the problem of guiding a fixed-wing UAV. Differently from the mentioned approaches, this work considers the full twelve-states coupled dynamics model of the UAV. The proposed strategy is based on two techniques to control the whole 6 DOF UAV. First, a feedback-linearization based controller is used to reduce the twelve states nonlinear model to a simplified linear model, using the generalized forces and moments as virtual control inputs. Second, a linear MPC is implemented to solve the trajectory tracking and control allocation problems simultaneously, ensuring feasibility between the virtual control inputs and the applied ones.

Simulations are performed using MATLAB software, and the results show that the proposed strategy is capable of guiding the UAV along a desired trajectory from any feasible initial configuration.

The remainder of this paper is structured as follows: in the next section, we present related works that deal with guidance problems. In section 3, the methodology of the proposed controller is developed. Simulation results are shown in section 4, and section 5 concludes the work.

⋆ This work was in part supported by the project INCT (National Institute of Science and Technology) under the grant CNPq (Brazilian National Research Council) 465755/2014-3, FAPESP (São Paulo Research Foundation), Brazil 2014/50851-0. This work was also supported in part by the Coordenação de Aperfeiçoamento de Pessoal de Nível Superior (CAPES), Brazil (Finance Code 88887.136349/2017-00, and 001), CNPq, Brazil (grant numbers 311063/2017-9, 313568/2017-0 and 426392/2016-7), and FAPEMIG, Brazil (grant number APQ-03090-17).

2. RELATED WORK

It is possible to find in the literature a great number of control techniques applied to the UAV guidance problem.

To begin with, (Kang and Hedrick, 2009) use a nonlinear MPC, in parallel with a set of low-level controllers, to transform the tracking problem into a regulation one. In the same subject, (Alessandretti and Aguiar, 2017) deal with the problem of path following of a fixed-wing UAV with an inner-outer loop design composed of a sampled-data MPC and low-level controllers, providing advantages like the reduction of computational burden.

In (Lesprier et al., 2015) a two stage control strategy is proposed for the longitudinal dynamics of the UAV. The first step consists of a classical pole placement method, followed by partially linearized inner loops and a robust $\mathcal{H}_\infty$ outer loop controller. On the feedback linearization subject, (Zhou et al., 2014) propose an attitude controller which also uses adaptive control to stabilize the decoupled model of the UAV.

Furthermore, in (Rezende et al., 2018) a robust control law, based on a reference model with constrained inputs and states, is proposed to navigate the UAV inside a smooth vector field in $\mathbb{R}^2$ and $\mathbb{R}^3$.

Also, (Raffo et al., 2010) design an integral predictive and nonlinear robust control strategy to solve the path following problem for a quadrotor helicopter in a hierarchical scheme, whilst a $\mathcal{H}_\infty$ controller stabilizes the rotational movements. Another $\mathcal{H}_\infty$ control approach is found on (Ferreira et al., 2011), where a secondary state feedback control is used to reject input disturbances.

Differently from the previous approaches, this work proposes an exact feedback-linearization controller for position and attitude control of a fixed-wing UAV, using the coupled nonlinear dynamics equations, and a MPC controller for the linearized system.

3. CONTROL STRATEGY

This section presents the development of the proposed control strategy. The details about fixed-wing UAV modelling such as dynamic equations and aerodynamics coefficients will not be covered here and can be found in (Stevens et al., 2015) and (Beard and McLain, 2012).

3.1 UAV Model

The nonlinear model of the UAV is presented in equations (1) - (4), where $p_n,\ p_e,\ p_d$ represent the north, east and down positions, $u,\ v,\ w$ the body velocities, $\phi,\ \theta,\ \psi$ the attitude (roll, pitch and yaw angles), and $p,\ q,\ r$ the angular velocities on the body-fixed frame of the UAV.

Furthermore, m is the UAV mass, Γ_i are combinations of the inertial moments (Beard and McLain, 2012), represented by J_{ik}, and $R_{a,b}$ represents the rotation matrix of b around the axis a.

The virtual control inputs $f_x,\ f_y,\ f_z$ represent the forces in the xyz body frame, and $l,\ m,\ n$ represent the moments.

$$\begin{pmatrix}\dot{p_n}\\ \dot{p_e}\\ \dot{p_d}\end{pmatrix} = R_{z,\psi}R_{y,\theta}R_{x,\phi}\begin{pmatrix}u\\ v\\ w\end{pmatrix}, \tag{1}$$

$$\begin{pmatrix}\dot{u}\\ \dot{v}\\ \dot{w}\end{pmatrix} = \begin{pmatrix}rv-qw\\ pw-ru\\ qu-pv\end{pmatrix} + \frac{1}{\mathsf{m}}\begin{pmatrix}f_x\\ f_y\\ f_z\end{pmatrix}, \tag{2}$$

$$\begin{pmatrix}\dot{\phi}\\ \dot{\theta}\\ \dot{\psi}\end{pmatrix} = \begin{pmatrix}1 & \sin\phi\tan\theta & \cos\phi\tan\theta\\ 0 & \cos\phi & -\sin\phi\\ 0 & \frac{\sin\phi}{\cos\theta} & \frac{\cos\phi}{\cos\theta}\end{pmatrix}\begin{pmatrix}p\\ q\\ r\end{pmatrix}, \tag{3}$$

$$\begin{pmatrix}\dot{p}\\ \dot{q}\\ \dot{r}\end{pmatrix} = \begin{pmatrix}\Gamma_1 pq - \Gamma_2 qr\\ \Gamma_5 pr - \Gamma_6(p^2-r^2)\\ \Gamma_7 pq - \Gamma_1 qr\end{pmatrix} + \begin{pmatrix}\Gamma_3 l - \Gamma_4 n\\ \frac{m}{J_{yy}}\\ \Gamma_4 l + \Gamma_8 n\end{pmatrix}. \tag{4}$$

The UAV is subjected to aerodynamic constraints, regarding flight speed and orientation with respect to the wind, allowing it to flight in stable conditions. These constraints are specifically for each UAV. We will deal with them in the next sections.

The relationship between the generalized forces and moments and the applied control signals on the UAV is given by (5), where $\delta_a, \delta_e, \delta_r$ represent the deflection of ailerons, elevators and rudder, respectively, and δ_t represents the throttle percentage.

$$\underbrace{\begin{bmatrix}f_x\\ f_y\\ f_z\\ l\\ m\\ n\end{bmatrix}}_{F} = M_{6\times4} \times \underbrace{\begin{bmatrix}\delta_a\\ \delta_e\\ \delta_r\\ \delta_t\end{bmatrix}}_{\vec{\mathbf{u}}} + \hat{C}_{6\times1}. \tag{5}$$

In equation (5), M is composed by the aerodynamics coefficients of the UAV control surfaces, and $\hat{C}$ is composed by the aerodynamics forces and moments generated by the fixed surfaces. These can be obtained from data tables, and depend on the angle of attack, sideslip angle, and from the UAV states.

Therefore, since M is not a square matrix, as long as $\det(M^T M) \neq 0$, we can obtain $\vec{\mathbf{u}}$ from $\hat{C}$ and a proper F as follows:

$$\vec{\mathbf{u}} = M^+(F - \hat{C}), \tag{6}$$

where M^+ is the Moore–Penrose left pseudo-inverse of M.

3.2 Problem Formulation

With the presented UAV model, we can now define the problem in which we are going to apply the control strategy developed in this work as follows:

Problem 1. Given a smooth reference trajectory ξ^d, find a set of admissible control inputs $\delta_a, \delta_e, \delta_r, \delta_t$ in order to guide the UAV along ξ^d, from any initial configuration.

Also, in order to validate the model and the proposed controller, we need the following assumptions:

A1. The UAV is flying at a constant speed;
A2. The reference trajectory ξ^d and all its time derivatives are defined and continuous;
A3. The pitch angle (θ) will remain within the valid range $|\theta| < \frac{\pi}{2}$.

In this work, we consider the task of tracking a trajectory given by a vector field, which leads to the circulation of a target curve. The structure of the vector field and the desired trajectory are presented in Section 4.

3.3 Feedback Linearization

In order to obtain a linearized system, we will use input-output feedback linearization (Khalil and Grizzle, 2002). With a change of variables, a nonlinear system

$$\begin{aligned} \dot{x} &= f(x) + g(x)\hat{u}, \\ y &= h(x), \end{aligned} \tag{7}$$

can be transformed to the normal form

$$\begin{aligned} \dot{\eta} &= f(\eta, \xi), \\ \dot{\xi} &= A\xi + B\gamma(\xi)[\hat{u} - \alpha(\xi)], \\ y &= C\xi, \end{aligned} \tag{8}$$

where $\dot{\eta}$ determines the system internal dynamics, and $\dot{\xi}$ determines the external dynamics.

Definition 1. (Khalil and Grizzle, 2002) An output of a nonlinear system has relative degree ρ_k if

$$L_{g_k} L_f^{i-1} h(x) = 0, L_{g_k} L_f^{\rho_k - 1} h(x) \neq 0, \forall i \in [1, \rho_k - 1]\,.$$

For MIMO systems, the relative degree ρ of the complete system will be given by the sum of all output's relative degrees ρ_k.

For the case where ρ equals the number of states, the internal dynamics is removed, yielding

$$\begin{aligned} \dot{\xi} &= A\xi + B\gamma(\xi)[\hat{u} - \alpha(\xi)], \\ y &= C\xi. \end{aligned} \tag{9}$$

It is possible then to use the control law $\hat{u} = \alpha(\xi) + \beta(\xi)\mathrm{v}$, with $\beta(\xi) = \gamma(\xi)^{-1}$, which leads to the linearized system

$$\begin{aligned} \dot{\xi} &= A\xi + B\mathrm{v}, \\ y &= C\xi. \end{aligned} \tag{10}$$

In this work, we choose the desired outputs as the three linear positions $[p_n, p_e, h]$, where $h = -p_d$, and the Euler angles $[\phi, \theta, \psi]$. Also, we choose the generalized forces and moments as the controls inputs ($\hat{u} = F$). This way, we have $\rho_k = 2, k = 1, ..., 6$ and $\rho = 12$, therefore we eliminate internal dynamics. Furthermore, according to (Khalil and Grizzle, 2002), $\alpha(\xi)$ and $\gamma(\xi)$ are given by

$$\gamma(\xi) = \begin{bmatrix} L_{g_1} L_f h_1(\xi) & \cdots & L_{g_6} L_f h_1(\xi) \\ L_{g_1} L_f h_2(\xi) & \cdots & L_{g_6} L_f h_2(\xi) \\ \vdots & \ddots & \vdots \\ L_{g_1} L_f h_6(\xi) & \cdots & L_{g_6} L_f h_6(\xi) \end{bmatrix}, \tag{11}$$

$$\alpha(\xi) = \gamma^{-1}(\xi) \begin{bmatrix} L_f^2 h_1(\xi) \\ L_f^2 h_2(\xi) \\ L_f^2 h_3(\xi) \\ L_f^2 h_4(\xi) \\ L_f^2 h_5(\xi) \\ L_f^2 h_6(\xi) \end{bmatrix} = \gamma^{-1}(\xi) b(\xi), \tag{12}$$

$$\beta(\xi) = \gamma^{-1}(\xi). \tag{13}$$

For the expanded version of these equations, please refer to appendix A.

Therefore, as long as $det(\gamma(\xi)) \neq 0$, we can choose

$$F = \alpha(\xi) + \beta(\xi)\mathrm{v}, \tag{14}$$

leading to the linearized system (10) with

$$\xi = \begin{bmatrix} p_n & \dot{p_n} & p_e & \dot{p_e} & h & \dot{h} & \phi & \dot{\phi} & \theta & \dot{\theta} & \psi & \dot{\psi} \end{bmatrix}^T, \tag{15}$$

$$A = \begin{bmatrix} A_1 & \mathbf{0} & \mathbf{0} & \mathbf{0} & \mathbf{0} & \mathbf{0} \\ \mathbf{0} & A_1 & \mathbf{0} & \mathbf{0} & \mathbf{0} & \mathbf{0} \\ \mathbf{0} & \mathbf{0} & A_1 & \mathbf{0} & \mathbf{0} & \mathbf{0} \\ \mathbf{0} & \mathbf{0} & \mathbf{0} & A_1 & \mathbf{0} & \mathbf{0} \\ \mathbf{0} & \mathbf{0} & \mathbf{0} & \mathbf{0} & A_1 & \mathbf{0} \\ \mathbf{0} & \mathbf{0} & \mathbf{0} & \mathbf{0} & \mathbf{0} & A_1 \end{bmatrix}, A_1 = \begin{bmatrix} 0 & 1 \\ 0 & 0 \end{bmatrix}, \tag{16}$$

$$B = \begin{bmatrix} B_1 & \mathbf{0} & \mathbf{0} \\ \mathbf{0} & B_1 & \mathbf{0} \\ \mathbf{0} & \mathbf{0} & B_1 \end{bmatrix}, B_1 = \begin{bmatrix} 0 & 0 \\ 1 & 0 \\ 0 & 0 \\ 0 & 1 \end{bmatrix}, \tag{17}$$

$$C = \begin{bmatrix} C_1 & \mathbf{0} & \mathbf{0} & \mathbf{0} & \mathbf{0} & \mathbf{0} \\ \mathbf{0} & C_1 & \mathbf{0} & \mathbf{0} & \mathbf{0} & \mathbf{0} \\ \mathbf{0} & \mathbf{0} & C_1 & \mathbf{0} & \mathbf{0} & \mathbf{0} \\ \mathbf{0} & \mathbf{0} & \mathbf{0} & C_1 & \mathbf{0} & \mathbf{0} \\ \mathbf{0} & \mathbf{0} & \mathbf{0} & \mathbf{0} & C_1 & \mathbf{0} \\ \mathbf{0} & \mathbf{0} & \mathbf{0} & \mathbf{0} & \mathbf{0} & C_1 \end{bmatrix}, C_1 = [1\ 0]\,, \tag{18}$$

where $\mathbf{0}$ are zeros matrices of appropriate size.

For the model presented in this paper, the condition $det(\gamma(\xi)) \neq 0$ will maintain as long as assumption **A3** holds.

3.4 Optimal Control

Since we are using the left pseudo-inverse, equation (6) only gives us the minimum quadratic error solution for arbitrary values of F. Therefore, we need to consider constraints on F. For that, suppose a virtual input F_1, that generates a control input $\overrightarrow{\mathbf{u}}_1$ as follows:

$$\overrightarrow{\mathbf{u}}_1 = M^+(F_1 - \hat{C}). \tag{19}$$

Since M^+ only gives the minimum quadratic error solution, the actual virtual input, F_2, generated by $\overrightarrow{\mathbf{u}}_1$, will be given by

$$F_2 = M \times \overrightarrow{\mathbf{u}}_1 + \hat{C}. \tag{20}$$

However, the feasible solution must ensure $F_2 = F_1 = F$. By replacing (19) in (20), we have

$$F = M \times M^+(F - \hat{C}) + \hat{C}. \tag{21}$$

Reorganizing (21), we find that if $(F - \hat{C})$ is in the null space of $(I - M \times M^+)$, we can ensure that $F_2 = F_1$ through

$$(I - M \times M^+)(F - \hat{C}) = 0. \tag{22}$$

Replacing the control law (14) in (22), we are able to relate the linear system control inputs with the UAV model control inputs, ensuring that feasible transformations between control inputs are achieved, as long as we choose v to respect the constraint

$$(I - M \times M^+)(\alpha(\xi) + \beta(\xi)\mathrm{v} - \hat{C}) = 0. \tag{23}$$

Furthermore, we also need v to respect the limits of $\overrightarrow{\mathbf{u}}$. We will do this by replacing (14) in (19)

$$\overrightarrow{\mathbf{u}}_{max} \geq M^+(\alpha(\xi) + \beta(\xi)\mathrm{v} - \hat{C}) \geq \overrightarrow{\mathbf{u}}_{min}. \tag{24}$$

From (24) we ensure that v must respect the bounds of $\overrightarrow{\mathbf{u}}$, and from (23) we ensure feasibility between virtual control inputs and the real ones.

Finally, our objective is to reduce the error of the linear system (10) with respect to a desired trajectory ξ^d. For

that, we propose an optimal control problem in the form of

$$J(v,\xi) = \min_{\mathrm{v}} \int_{t_0}^{t_f} (\xi-\xi^d)^T Q(\xi-\xi^d) + \mathrm{v}^T R \mathrm{v}\ dt + (\xi_N - \xi_N^d)^T P(\xi_N - \xi_N^d) \quad s.t. (10),(23),(24) \tag{25}$$

where Q and R are the states and controls weighting matrices, respectively, and P is the terminal cost weighting matrix. In order to improve convergence, we will use the incremental MPC framework to solve the quadratic optimal control problem. Then, the linear control input is given by

$$\mathrm{v}_k = \mathrm{v}_{k-1} + \Delta \mathrm{v}_k. \tag{26}$$

Finally, the system (10) can be written in the discrete time and incremental form as follows:

$$\underbrace{\begin{bmatrix}\xi_{k+1}\\ \mathrm{v}_k\end{bmatrix}}_{\bar{\xi}^+} = \underbrace{\begin{bmatrix}A_d & B_d\\ \mathbf{0} & I\end{bmatrix}}_{\bar{A}} \underbrace{\begin{bmatrix}\xi_k\\ \mathrm{v}_{k-1}\end{bmatrix}}_{\bar{\xi}} + \underbrace{\begin{bmatrix}B_d\\ I\end{bmatrix}}_{\bar{B}} \Delta \mathrm{v}_k. \tag{27}$$

where A_d and B_d are obtained by discretizing A and B, respectively, using Zero-order Hold (ZoH).

Furthermore, we will consider constraints on the rate of the control inputs. Replacing (26) in (6) with (14), we obtain

$$\overrightarrow{\mathbf{u}}_k = M^+(\alpha(\xi_k) + \beta(\xi_k)(\mathrm{v}_{k-1} + \Delta \mathrm{v}_k) - \hat{C}). \tag{28}$$

Using the superposition principle we can analyse the effects of $\Delta \mathrm{v}_k$ in $\overrightarrow{\mathbf{u}}_k$:

$$\Delta \overrightarrow{\mathbf{u}}_k = M^+ \beta(\xi_k) \Delta \mathrm{v}_k, \tag{29}$$

where $\Delta \overrightarrow{\mathbf{u}}_k$ is the corresponding change in $\overrightarrow{\mathbf{u}}_k$ due to $\Delta \mathrm{v}_k$. This way, we can consider the constraints in $\Delta \mathrm{v}_k$ as

$$|M^+ \beta(\xi_k) \Delta \mathrm{v}_k| \leq \Delta \overrightarrow{\mathbf{u}}_{max}. \tag{30}$$

Finally, defining $\hat{\xi}_j = \bar{\xi}_{k+j|k} - \bar{\xi}^d_{k+j|k}$ and $\Delta \mathrm{v}_j = \Delta \mathrm{v}_{k+j|k}$, we can rewrite the optimal control problem as

$$J(\Delta v, \hat{\xi}_j) = \min_{\Delta \mathrm{v}} \sum_{j=0}^{N-1} \left[\hat{\xi_j}^T Q \hat{\xi_j} + {\Delta \mathrm{v}_j}^T R \Delta \mathrm{v}_j\right] + \hat{\xi}_N^T P \hat{\xi}_N. \tag{31}$$

$$s.t.\ (27),$$
$$(I - M \times M^+)(\alpha(\xi_{k|k}) + \beta(\xi_{k|k})(\mathrm{v}_{j-1} + \Delta \mathrm{v}_j) - \hat{C}) = 0,$$
$$M^+(\alpha(\xi_{k|k}) + \beta(\xi_{k|k}))(\mathrm{v}_{j-1} + \Delta \mathrm{v}_j) - \hat{C}) \leq \overrightarrow{\mathbf{u}}_{max},$$
$$M^+(\alpha(\xi_{k|k}) + \beta(\xi_{k|k}))(\mathrm{v}_{j-1} + \Delta \mathrm{v}_j) - \hat{C}) \geq \overrightarrow{\mathbf{u}}_{min},$$
$$|M^+ \beta(\xi_{k|k}) \Delta \mathrm{v}_j| \leq \Delta \overrightarrow{\mathbf{u}}_{max},$$
$$|\theta_j| < \frac{\pi}{2}.$$

The states constraints on θ are added in order to ensure that $det(\gamma(\xi)) \neq 0$, aiming to keep the UAV in stable flight conditions. Also, $\alpha(\xi_{k+j|k})$ and $\beta(\xi_{k+j|k})$ are calculated in $j = 0$ and kept constant through the prediction horizon.

For the MPC formulation, we need to choose the prediction horizon (N_p) and the control horizon (N_u). A commonly used strategy is to select $N_p = N_u$, but selecting a smaller N_u provides some advantages like faster computations, as it reduces the number of decision variables.

Propagating (27) through the prediction horizon, we obtain

$$\boldsymbol{\xi}^+ = T\bar{\xi}_k + S\bar{u}, \tag{32}$$

where T is $N_p \times 12$ and S is $N_p \times N_u$, given as follows

$$\boldsymbol{\xi}^+ = \begin{bmatrix}\bar{\xi}_{k+1}\\ \bar{\xi}_{k+2}\\ \vdots\\ \bar{\xi}_{k+N_p}\end{bmatrix}, \qquad T = \begin{bmatrix}\bar{A}\\ \bar{A}^2\\ \vdots\\ \bar{A}^{N_p}\end{bmatrix},$$

$$S = \begin{bmatrix}\bar{B} & \mathbf{0} & \cdots & \mathbf{0}\\ \bar{A}\bar{B} & \bar{B} & \cdots & \mathbf{0}\\ \vdots & \vdots & \ddots & \vdots\\ \bar{A}^{N_p-1}\bar{B} & \bar{A}^{N_p-2}\bar{B} & \cdots & \sum_{i=1}^{N_p-N_u} \bar{A}^i \bar{B}\end{bmatrix},$$

$$\bar{u} = \begin{bmatrix}\Delta \mathrm{v}_k\\ \Delta \mathrm{v}_{k+1}\\ \vdots\\ \Delta \mathrm{v}_{k+N_u-1}\end{bmatrix}. \tag{33}$$

Finally, the optimal control problem is reduced to

$$J(\bar{u}, \bar{\xi}_k) = \min_{\bar{u}} \frac{1}{2}\bar{u}^T H \bar{u} + f^T \bar{u} + \frac{1}{2} Y, \quad s.t.\ G\bar{u} \leq W,\ E\bar{u} = Z, \tag{34}$$

with

$$H = 2(\bar{R} + S^T \bar{Q} S), \tag{35}$$
$$f^T = 2(T\bar{\xi}_k - \bar{\xi}^d)^T \bar{Q} S, \tag{36}$$
$$Y = (T\bar{\xi}_k - \bar{\xi}^d)^T \bar{Q}(T\bar{\xi}_k - \bar{\xi}^d) + \bar{\xi}_k^T Q \bar{\xi}_k, \tag{37}$$

where $\bar{Q} = blkdiag(Q, Q, ..., P)$, $\bar{R} = blkdiag(R, R, ..., R)$, and $\bar{\xi}^d = [\xi_k^{d^T}, ..., \xi_{k+N_p-1}^{d^T}]^T$. Also, G, W, E, and Z are given in appendix B.

4. RESULTS

The proposed strategy is applied in a task of tracking a trajectory given by a vector field which leads to the circulation of a trajectory curve defined implicitly. Simulation results are performed in MATLAB software.

The vector field used in this work is proposed in (Gonçalves et al., 2010). Briefly, let n be the dimension of the workspace and $\mathbf{p} \in \mathbb{R}^n$ a coordinate for this space. The implementation relies on finding $n-1$ well-behaved scalar functions $\eta_1(\mathbf{p}), ..., \eta_{n-1}(\mathbf{p})$, such that the intersections of these functions $\eta_i(\mathbf{p}) = 0, i = 1, 2, ..., n-1$ define the target curve ζ. We are using vector fields in $\mathbb{R}^3$, where their structure is given by

$$\Omega(p_e, p_n, h) = G(P)\frac{\nabla P}{||P||} + H(P)\frac{\nabla \eta_1 \times \nabla \eta_2}{||\nabla \eta_1 \times \nabla \eta_2||}, \tag{38}$$

where P gives an idea of distance to the desired curve ζ, $G(P) : \mathbb{R}^3 \to \mathbb{R}$ is a scalar function such that $G(P) = 0 \iff P = 0$, $H(P)$ is defined as $H(P) = \sqrt{1 - G(P)^2}$, and $\nabla \eta_1 \times \nabla \eta_2$ defines a term tangent to the curve.

The following parameters are used in the simulations to generate the field: $\eta_1 = h + \mu(\epsilon^{-2} p_e^2 - 1)$, $\eta_2 = \sigma^{-2} p_n^2 + \epsilon^{-2} p_e^2 - 1$, with $\mu = 50$, $\sigma = 600$ and $\epsilon = 500$. These parameters represent the intersection of an ellipse with main axis given by σ and ϵ, and a parable defined by μ and ϵ.

The relationship between the components of the vector field Ω and the desired trajectory ξ^d at time k is given by equations (39)-(48).

$$\xi_k^d = [p_n^d \ \lambda p_n^d \ p_e^d \ \lambda p_e^d \ h^d \ \lambda h^d \ \phi^d \ \lambda\phi^d \ \theta^d \ \lambda\theta^d \ \psi^d \ \lambda\psi^d] \quad (39)$$

$$\lambda p_n^d = \cos(\Omega_\psi) V_{ref}, \qquad p_n^d = p_{n_k} + \lambda p_n^d \Delta_\tau, \quad (40)$$

$$\lambda p_n^d = \sin(\Omega_\psi) V_{ref}, \qquad p_e^d = p_{e_k} + \lambda p_e^d \Delta_\tau, \quad (41)$$

$$\lambda h^d = 3\Omega_z, \qquad h^d = h_k + \lambda h^d \Delta_\tau, \quad (42)$$

$$\lambda\phi^d = \tanh\left(\frac{\frac{1}{6}\lambda\psi^d - \phi_k}{\Delta_\tau}\right), \qquad \phi^d = \phi_k + \lambda\phi^d \Delta_\tau, \quad (43)$$

$$\lambda\theta^d = \tanh\left(\frac{\Omega_\theta - \theta_k}{\Delta_\tau}\right), \qquad \theta^d = \theta_k + \lambda\theta^d \Delta_\tau, \quad (44)$$

$$\lambda\psi^d = \tanh\left(\frac{\Omega_\psi - \psi_k}{\Delta_\tau}\right), \qquad \psi^d = \psi_k + \lambda\psi^d \Delta_\tau, \quad (45)$$

$$\Omega_{xy} = \sqrt{\Omega_x^2 + \Omega_y^2}, \quad (46)$$

$$\Omega_\psi = atan2(\Omega_x, \ \Omega_y), \quad (47)$$

$$\Omega_\theta = atan2(\Omega_z, \ \Omega_{xy}), \quad (48)$$

where $\Omega_x, \Omega_y, \Omega_z$ are the vector field components in the xyz plane, V_{ref} is the reference speed in the xy plane, Δ_τ is the sampling time, and $\lambda(\cdot)$ stands for the discrete derivative. To extend the desired trajectory over the prediction horizon $[k+1, ..., k+N_p-1]$, we need to integrate the vector field. This way, the resulting field at time $k+i$ will be given by $\Omega(p^d_{e_{k+i-1}}, p^d_{n_{k+i-1}}, h^d_{k+i-1})$ and ξ^d_{k+i} is calculate as in (39). Finally, the complete reference vector is given by

$$\bar{\xi}^d = \begin{bmatrix} \xi_k^{d^T} & \xi_{k+1}^{d^T} & \cdots & \xi_{k+N_p-1}^{d^T} \end{bmatrix}^T. \quad (49)$$

Table 1 shows the effects of different N_p values on the final cost and execution time. The first two columns show the values of N_u and N_p. Column three shows the average execution time of the algorithm, while column four shows the percentage increase with respect to the first row. Columns five and six show the total cost (J) and the percentage reduction with respect to the first row.

Table 1. Selection of N_p.

N_u	N_p	Time (s)	Increasing	Cost	Reduction
2	4	0.0053	-	9.3456e+05	-
2	6	0.0063	18,9%	7.4292e+05	20,5%
2	8	0.0072	35,8%	6.1254e+05	34,5%
2	10	0.0080	50,9%	5.7012e+05	39,0%
2	12	0.0095	79,2%	5.5506e+05	40,6%

From it, we can note that when increasing N_p beyond $N_p = 10$ there is almost no improvement on cost reduction, while the execution time keeps increasing, indicating that increasing N_p would imply in higher computational effort, without improving the results. Therefore, we have selected $N_u = 2$ and $N_p = 10$ for the simulations results.

The weighting matrices Q and R were tuned in order to emphasize the orientation error, regarding the field and control smoothness, leading to

$$Q_\xi = diag(0.1\ 1\ 0.1\ 1\ 0.1\ 1\ 5\ 15\ 5\ 15\ 5\ 15), \quad (50)$$

$$Q_v = diag(0\ 0\ 0\ 0\ 0\ 0), \quad (51)$$

$$Q = \begin{bmatrix} Q_\xi & \mathbf{0} \\ \mathbf{0} & Q_v \end{bmatrix}, \quad (52)$$

$$R = diag(10\ 10\ 10\ 5\ 5\ 5). \quad (53)$$

With Q and R we can select P as the solution of the algebraic Riccati equation from the LQR problem.

Furthermore, since M and $\hat{C}$ are estimated using the coefficient buildup method, we add parameter uncertainty to the simulations in order to verify the robustness of the strategy.

The UAV initial conditions are set to

$$\xi_0 = [0\ 0\ 250\ 23\ 0\ 0\ 0\ 0\ \frac{\pi}{2}\ 0\ 0\ 0\ 0\ 0\ 0\ 0\ 0.4]. \quad (54)$$

Finally, we have chosen a fixed reference speed V_{ref} for the UAV as 23m/s.

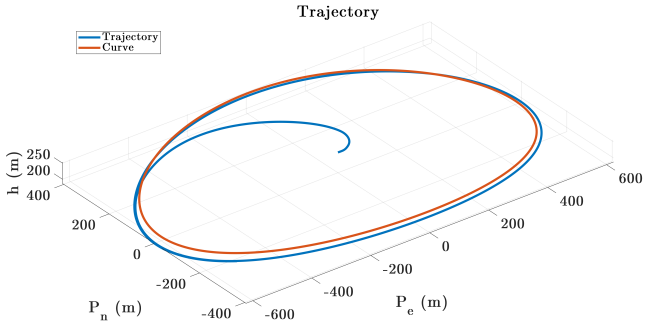

Figure 1. Trajectory executed by the UAV and the desired curve.

Figure 1 shows the trajectory executed by the UAV, for the nominal parameters, and the desired curve. Note that the UAV starts in the middle of the curve, and rapidly converges to it. North, East and Down positions are presented in Figure 2, where we can observe the effect of parameter variation on the UAV trajectory. Figure 3

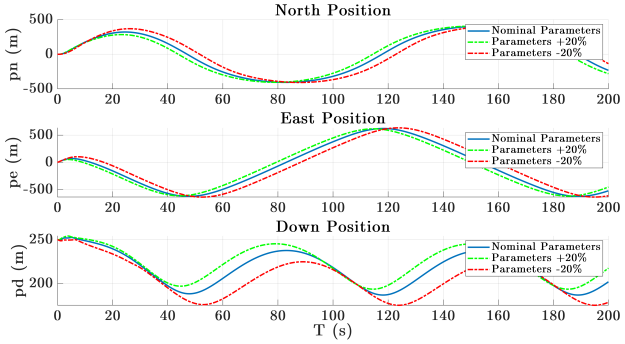

Figure 2. North, east and down positions of the UAV over the trajectory.

shows the error on roll, pitch and yaw angles. We can observe that despite of the different trajectories on xyz presented in Figure 2, the UAV orientation still converges to the field, presenting a maximum steady error of 0.01 rad. Furthermore, Figure 4 shows the control inputs. We

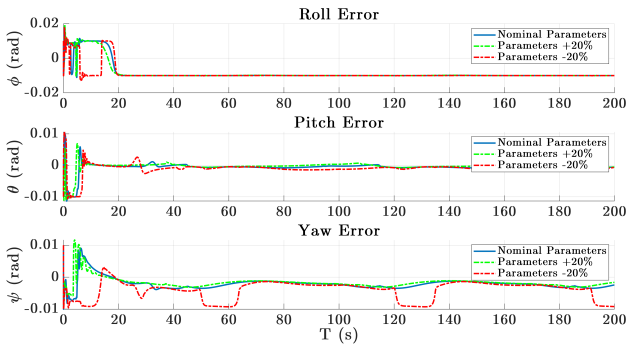

Figure 3. Error on roll, pitch and yaw angles during simulation.

can observe that parameter variation directly affects the control signals as a -20% variation on M coefficients leads to a higher control effort, whereas a +20% variation reduces the control effort. This is an expected behavior,

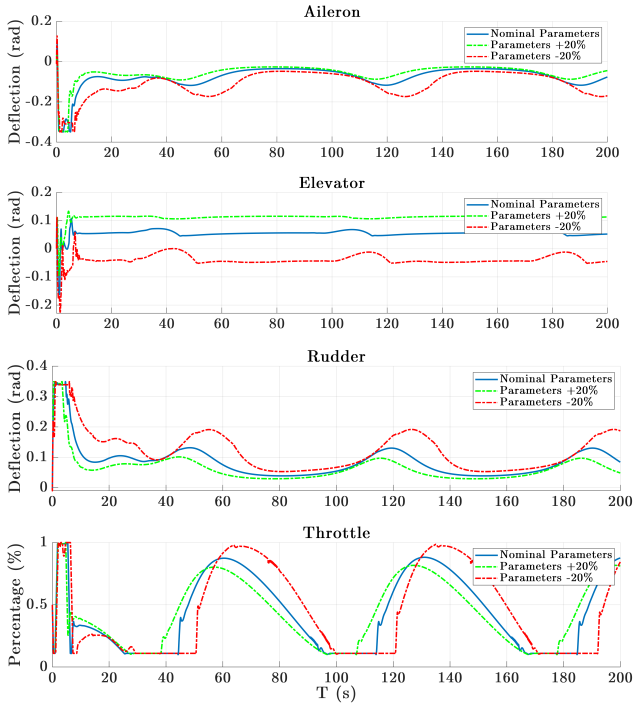

Figure 4. Applied control signals.

since M maps the control inputs into forces and moments. Therefore, smaller coefficients leads to higher control effort to produce the desired forces and moments. The same analysis applies to the opposite situation.

Finally, we compare the proposed strategy with the one presented in (Rezende et al., 2018), which uses a low level PID to simplify the complex 12 states model. Figure 5 shows the UAV alignment error ($|\psi - \Omega_\psi|$) for both strategies. We can observe that the proposed controller not only converges faster, but presents a smaller mean error (0.0099 rad against 0.1023 rad).

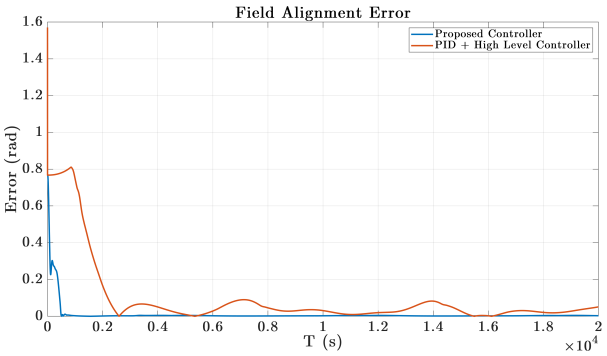

Figure 5. UAV alignment error with respect to the field.

5. CONCLUSION

This paper dealt with the problem of fixed-wing UAV guidance. A feedback-linearization based controller combined with linear MPC was proposed and the implementation of the strategy was presented and discussed. Different from the commonly found approaches in literature, the developed controller deals with the full coupled dynamics of the system, which avoids restrictions whereas controlling all 6 DOF of the UAV. Simulation results have shown the efficacy of the proposed strategy and the behavior of the prediction horizon in the tracking performance. Furthermore, the robustness of the controller against parameter uncertainties was verified by applying ±20% uncertainty on the coefficients.

As future work, we intend to implement the proposed controller in a hardware-in-the-loop system to evaluate the feasibility of implementing it on a small UAV. Furthermore, we also intend to use a tube-based MPC in order to improve robustness. We also intend to develop the proof of stability for the proposed strategy.

REFERENCES

Alessandretti, A. and Aguiar, A.P. (2017). A planar path-following model predictive controller for fixed-wing unmanned aerial vehicles. In *2017 11th International Workshop on Robot Motion and Control (RoMoCo)*, 59–64. IEEE.

Beard, R.W., Ferrin, J., and Humpherys, J. (2014). Fixed wing uav path following in wind with input constraints. *IEEE Transactions on Control Systems Technology*, 22(6), 2103–2117.

Beard, R.W. and McLain, T.W. (2012). *Small unmanned aircraft: Theory and practice*. Princeton university press.

Espinoza, T., Dzul, A., Lozano, R., and Parada, P. (2014). Backstepping-sliding mode controllers applied to a fixed-wing uav. *Journal of Intelligent & Robotic Systems*, 73(1-4), 67–79.

Ferreira, H.C., Baptista, R.S., Ishihara, J.Y., and Borges, G.A. (2011). Disturbance rejection in a fixed wing uav using nonlinear $\mathcal{H}_\infty$ state feedback. In *2011 9th IEEE International Conference on Control and Automation (ICCA)*, 386–391. IEEE.

Garcia-Baquero, L., Esteban, S., and Raffo, G. (2018). Singular perturbation control for the longitudinal and lateral-directional flight dynamics of a uav. In *IFAC Workshop on Networked & Autonomous Air & Space Systems NAASS 2018*, 124 – 129.

Gonçalves, V.M., Pimenta, L.C., Maia, C.A., Dutra, B.C., and Pereira, G.A. (2010). Vector fields for robot navigation along time-varying curves in n-dimensions. *IEEE Transactions on Robotics*, 26(4), 647–659.

Kang, Y. and Hedrick, J.K. (2009). Linear tracking for a fixed-wing uav using nonlinear model predictive control. *IEEE Transactions on Control Systems Technology*, 17(5), 1202–1210.

Khalil, H.K. and Grizzle, J.W. (2002). *Nonlinear systems*, volume 3. Prentice hall Upper Saddle River, NJ.

Lesprier, J., Biannic, J.M., and Roos, C. (2015). Modeling and robust nonlinear control of a fixed-wing uav. In *2015 IEEE Conference on Control Applications (CCA)*, 1334–1339. IEEE.

Raffo, G.V., Ortega, M.G., and Rubio, F.R. (2010). An integral predictive/nonlinear $\mathcal{H}_\infty$ control structure for a quadrotor helicopter. *Automatica*, 46(1), 29–39.

Rezende, A.M., Gonçalves, V.M., Raffo, G.V., and Pimenta, L.C. (2018). Robust fixed-wing uav guidance with circulating artificial vector fields. In *2018 IEEE/RSJ International Conference on Intelligent Robots and Systems (IROS)*, 5892–5899. IEEE.

Stevens, B.L., Lewis, F.L., and Johnson, E.N. (2015). *Aircraft control and simulation: dynamics, controls design, and autonomous systems*. John Wiley & Sons.

Zhou, W., Yin, K., Wang, R., and Wang, Y.E. (2014). Design of attitude control system for uav based on feedback linearization and adaptive control. *Mathematical Problems in Engineering*, 2014, 1–8.

Appendix A. FEEDBACK LINEARIZATION EQUATIONS

Here we expand the matrices $\gamma(\xi)$ and $b(\xi)$ from (13) for the specific case of this work, where i, j represent the row and column number, respectively.

For γ we have the following terms:

$$\gamma_{1,1} = \cos(\psi)\cos(\theta), \tag{A.1}$$
$$\gamma_{1,2} = -\sin(\psi)\cos(\phi) + \cos(\psi)\sin(\theta)\sin(\phi), \tag{A.2}$$
$$\gamma_{1,3} = \sin(\psi)\sin(\phi) + \cos(\psi)\sin(\theta)\cos(\phi), \tag{A.3}$$
$$\gamma_{1,4} = \gamma_{1,5} = \gamma_{1,6} = 0, \tag{A.4}$$
$$\gamma_{2,1} = \sin(\psi)\cos(\theta), \tag{A.5}$$
$$\gamma_{2,2} = \cos(\psi)\cos(\phi) + \sin(\psi)\sin(\theta)\sin(\phi), \tag{A.6}$$
$$\gamma_{2,3} = -\cos(\psi)\sin(\phi) + \sin(\psi)\sin(\theta)\cos(\phi), \tag{A.7}$$
$$\gamma_{2,4} = \gamma_{2,5} = \gamma_{2,6} = 0, \tag{A.8}$$
$$\gamma_{3,1} = -\sin(\theta), \tag{A.9}$$
$$\gamma_{3,2} = \cos(\theta)\sin(\phi), \tag{A.10}$$
$$\gamma_{3,3} = \cos(\theta)\cos(\phi), \tag{A.11}$$
$$\gamma_{3,4} = \gamma_{3,5} = \gamma_{3,6} = 0, \tag{A.12}$$
$$\gamma_{4,1} = \gamma_{4,2} = \gamma_{4,3} = 0, \tag{A.13}$$
$$\gamma_{4,4} = \frac{\cos(\phi)\sin(\theta)\,J_{xz} + J_{zz}\cos(\theta)}{\cos(\theta)\left(J_{xx}\,J_{yy} - {J_{xy}}^2\right)}, \tag{A.14}$$
$$\gamma_{4,5} = \frac{\sin(\phi)\sin(\theta)}{J_{yy}\cos(\theta)}, \tag{A.15}$$
$$\gamma_{4,6} = \frac{\cos(\phi)\sin(\theta)\,J_{xx} + J_{xz}\cos(\theta)}{\cos(\theta)\left(J_{xx}\,J_{yy} - {J_{xy}}^2\right)}, \tag{A.17}$$
$$\gamma_{5,1} = \gamma_{5,2} = \gamma_{5,3} = 0, \tag{A.18}$$
$$\gamma_{5,4} = -\frac{\sin(\phi)\,J_{xz}}{J_{xx}\,J_{yy} - {J_{xy}}^2}, \tag{A.19}$$
$$\gamma_{5,5} = \frac{\cos(\phi)}{J_{yy}}, \tag{A.20}$$
$$\gamma_{5,6} = -\frac{\sin(\phi)\,J_{xx}}{J_{xx}\,J_{yy} - {J_{xy}}^2}, \tag{A.21}$$
$$\gamma_{6,1} = \gamma_{6,2} = \gamma_{6,3} = 0, \tag{A.22}$$
$$\gamma_{6,4} = \frac{\cos(\phi)\,J_{xz}}{\cos(\theta)\left(J_{xx}\,J_{yy} - {J_{xy}}^2\right)}, \tag{A.23}$$
$$\gamma_{6,5} = \frac{\sin(\phi)}{\cos(\theta)\,J_{yy}}, \tag{A.24}$$
$$\gamma_{6,6} = \frac{\cos(\phi)\,J_{xx}}{\cos(\theta)\left(J_{xx}\,J_{yy} - {J_{xy}}^2\right)}. \tag{A.25}$$

For b we have the following elements:

$$b_1 = b_2 = b_3 = 0, \tag{A.26}$$
$$\begin{aligned} b_4 = &-2\left(\cos(\phi)\right)^2 qr - \cos(\phi)\sin(\phi)\,q^2 + \cos(\phi)\sin(\phi)\,r^2 \\ &+ \frac{\sin(\theta)\left(\cos(\phi)\,pq\Gamma_7 - \cos(\phi)\,qr\Gamma_1 - \sin(\phi)\,p^2\Gamma_6\right)}{\cos(\theta)} \\ &+ \frac{\sin(\theta)\left(\sin(\phi)\,pr\Gamma_5 + \sin(\phi)\,r^2\Gamma_6 + \cos(\varphi)\,pq\right)}{\cos(\theta)} \\ &- \frac{\sin(\phi)\sin(\theta)\,pr}{\cos(\theta)} + pq\Gamma_1 - qr\Gamma_2 + 4\,\frac{\left(\cos(\phi)\right)^2 qr}{\left(\cos(\theta)\right)^2} \\ &+ 2\,\frac{\sin(\varphi)\left(q^2 - 2\,r^2\right)\cos(\varphi) + qr\left(\left(\cos(\theta)\right)^2 - 2\right)}{\left(\cos(\theta)\right)^2}, \end{aligned} \tag{A.27}$$
$$\begin{aligned} b_5 = &\frac{\cos(\phi)\left(-2\sin(\phi)\,qr + \left(q^2 - r^2\right)\cos(\phi)\right)\sin(\theta)}{\cos(\theta)} \\ &\left(-p^2\Gamma_6 + pr\Gamma_5 + r^2\Gamma_6\right)\cos(\varphi) - \sin(\varphi)\,q\left(p\Gamma_7 - r\Gamma_1\right) \\ &- \cos(\phi)\,pr - \sin(\phi)\,pq - \frac{\sin(\theta)\,q^2}{\cos(\theta)}, \end{aligned} \tag{A.28}$$
$$\begin{aligned} b_6 = &2\,\frac{\sin(\theta)\cos(\phi)\left(\left(q^2 - r^2\right)\sin(\phi) + 2\cos(\phi)\,qr\right)}{\left(\cos(\theta)\right)^2} \\ &\frac{\cos(\phi)\,q\left(p\Gamma_7 - r\Gamma_1 + p\right)}{\cos(\theta)} - 2\,\frac{\sin(\theta)\,qr}{\left(\cos(\theta)\right)^2} \\ &- \frac{\left(-r^2\Gamma_6 - p\left(\Gamma_5 - 1\right)r + p^2\Gamma_6\right)\sin(\phi)}{\cos(\theta)}. \end{aligned} \tag{A.29}$$

Appendix B. CONSTRAINT MATRICES

Here we presented the constraint matrices from the optimal control problem (34).

$$E = \begin{bmatrix} E_{1,1} & E_{1,2} & \cdots & E_{1,N_u} \\ E_{2,1} & E_{2,2} & \cdots & E_{2,N_u} \\ \vdots & \vdots & \ddots & \vdots \\ E_{N_p,1} & E_{N_p,2} & \cdots & E_{N_p,N_u} \end{bmatrix}, Z = \begin{bmatrix} Z_1 \\ Z_2 \\ \vdots \\ Z_{N_p} \end{bmatrix}, \quad \text{(B.1)}$$

$$G = \begin{bmatrix} G_{1,1} & G_{1,2} & \cdots & G_{1,N_u} \\ G_{2,1} & G_{2,2} & \cdots & G_{2,N_u} \\ \vdots & \vdots & \ddots & \vdots \\ G_{N_p,1} & G_{N_p,2} & \cdots & G_{N_p,N_u} \end{bmatrix}, W = \begin{bmatrix} W_1 \\ W_2 \\ \vdots \\ W_{N_p} \end{bmatrix}, \quad \text{(B.2)}$$

$$E_{i,j} = \begin{cases} \mathbf{0}, & j \neq i \\ (I - M \times M^+)\beta(\bar{\xi}_k), & j = i \end{cases}, \quad \text{(B.3)}$$

$$Z_i = (I - M \times M^+)(\alpha(\bar{\xi}_k) + \beta(\bar{\xi}_k)v_k - \hat{C}), \quad \text{(B.4)}$$

$$G_{i,j} = \begin{cases} \mathbf{0}, & j > i \\ \begin{bmatrix} (I - M \times M^+)\beta(\bar{\xi}_k) \\ -(I - M \times M^+)\beta(\bar{\xi}_k) \\ \mathcal{I}_\theta A^{i-j} B \\ -\mathcal{I}_\theta A^{i-j} B \end{bmatrix}, & j \leq i \end{cases}, \quad \text{(B.5)}$$

$$W_i = \begin{bmatrix} \Delta \overrightarrow{\mathbf{u}}_{max} \\ -\Delta \overrightarrow{\mathbf{u}}_{min} \\ \overrightarrow{\mathbf{u}}_{max} - M^+(\alpha(\bar{\xi}_k) + \beta(\bar{\xi}_k)v_k - \hat{C}) \\ -\overrightarrow{\mathbf{u}}_{min} + M^+(\alpha(\bar{\xi}) + \beta(\bar{\xi}_k)v_k - \hat{C}) \\ \pi/2 - \mathcal{I}_\theta A^i \xi_k \\ \pi/2 + \mathcal{I}_\theta A^i \xi_k \end{bmatrix}, \quad \text{(B.6)}$$

$$\mathcal{I}_{\theta_i} = \begin{cases} 0, & i \neq 9 \\ 1, & i = 9 \end{cases}, i \in [0, ..., 18]. \quad \text{(B.7)}$$